Remote Sensing Applications: Society and Environment 37 (2025) 101509

Contents lists available at ScienceDirect

Remote Sensing Applications: Society and Environment

journal homepage: www.elsevier.com/locate/rsase

Protected agriculture mapping at continental scale for highlighting hotspots of altered hydrological processes

Daniele la Cecilia [a,*], Francesca Despini [b]

[a] Department of Civil Environmental and Architectural Engineering, University of Padua, Italy
[b] Department of Engineering Enzo Ferrari, University of Modena and Reggio Emilia, Italy

ARTICLE INFO

Keywords:
Protected agriculture
Plastic greenhouse
OPAC
Sentinel-2
Random forest

ABSTRACT

The presence of agricultural catchments used for protected agriculture is growing worldwide. Monitoring studies document regional-scale and long-term impacts of widespread greenhouse horticulture production on the hydrological cycle, agricultural chemicals fate, and plastic pollution. Still, methodological tools that allow for continuous and continental mapping of greenhouses are lacking. In this study, we present one such tool developed upon integrating an improved version of the random forest-based Open field and Protected Agriculture land cover Classifier (OPAC), of Sentinel-2 L2A data, with the computational power and storage capability of the Google Earth Engine (GEE) platform. The GEE platform allowed for (1) exploiting a recently deployed state-of-the-art cloud mask, (2) performing a time series analysis-based image aggregation step to generate an optimal scene to classify, while preserving the coherent information of each pixel in the collection and (3) integrating user-defined masks. The tool was applied at the pan-European level constrained on agricultural areas mapped in the CORINE Land Cover 2018 product. Against manually selected ground-truth pixels, OPAC achieved an overall accuracy of 92 % for the class of protected agriculture. The study reveals that in the summer period of 2019, protected agriculture covered 5300 km^2 of the pan-European agricultural area. The largest extensions of protected agriculture were in Turkey, Spain and Italy. The output land cover map can reveal locations where protected agriculture is altering the hydrological cycle and agricultural contaminants' fate in the environment as well as it can reveal potential sources of plastic pollution. The exploitation of the output map can thus expand the capability of modeling tools used for evaluating scenario analyses aiming to achieve a sustainable management of agricultural catchments.

1. Introduction

Greenhouse horticultural production enables high yields under a wide range of climatic conditions ranging from wet, cold and light-scarce areas (Badji et al., 2022; Achour et al., 2021) to dry, hot and light-abundant areas (Goddek et al., 2023) when combined with appropriate technological adaptations. Inside a greenhouse, farmers can modify local environmental factors to realize optimal crop growth conditions. Greenhouse horticulture falls under the umbrella of "protected agriculture", as compared to "open field agriculture" precisely for the possibility to control indoor conditions. In the meantime, climate change is driving weather-related crop

* Corresponding author. Department of Civil Environmental and Architectural Engineering University of Padua 35131, Padua, Italy.
E-mail address: daniele.lacecilia@unipd.it (D. la Cecilia).

https://doi.org/10.1016/j.rsase.2025.101509
Received 7 November 2024; Received in revised form 29 January 2025; Accepted 25 February 2025
Available online 26 February 2025

losses through more severe and frequent hazardous meteorological phenomena as well as increased seasonal climatic variability (Wade et al., 2022). The possibility to control the indoor climate has the additional environmental benefit of reducing crop transpiration. Fernández et al., (2010) show that the reference evapotranspiration (ET) under plastic greenhouses compared to open field conditions reached just 1 mm/day instead of 1.5 mm/day in winter and 4 mm/day rather than 6.5 mm/day in summer in Almeria, Spain. The lower ET in greenhouses compared to open fields is favoured by an ensemble of factors including the reduced solar radiation thanks to the use of the plastic roof (radiation transmission of about 60%–70%), further reduced with the application of whitening paint (radiation transmission of about 25%–50%) (Baille et al., 2001; Fernández et al., 2010), the higher relative humidity and the lower wind speed. Inherently, the lower crop transpiration reduces the need for irrigation water. This is relevant for improving the sustainability of food production given that agriculture is the sector that uses the largest share of water achieving values up to 90% (AQUASTAT, 2020). However, greenhouses inherently increase the imperviousness of agricultural catchment. In fact, current Sentinel-2-based land use land cover (LULC) maps classify greenhouses as "built-up" (Dynamic World by Brown et al., 2022). Moreover, in some areas the increased imperviousness is causing a local increase in fast runoff and flooding risk due to the delivery of rainfall directly into agricultural drainage channels (i.e., Campania region, Italy) (la Cecilia et al., 2024). Other countries mandated to harvest rainwater for irrigation purposes and mitigate water scarcity (i.e., The Netherlands and Spain). Inherently, rainwater harvesting and channelization both reduce aquifer recharge, whereas aquifers are often exploited as a source of irrigation water (Garcia-Caparros et al., 2017; Zhou et al., 2021). This can have implications on the health of groundwater-connected ecosystems (Jägermeyr et al., 2017).

Greenhouse horticulture is an anthropic LULC. Depending on management, agriculture can play a pivotal role in protecting and enhancing biodiversity and ecosystems, which further support services crucial for human well-being (Rey Benayas and Bullock, 2012; Duru et al., 2015). For example, natural and semi-natural grasslands (Bullock et al., 2011; Schils et al., 2022) are rich in biodiversity (Habel et al., 2013), contribute to livestock grazing (Erb et al., 2016) and constitute cultural heritage (Filippa et al., 2022). In contrast, the expansion of intensive agricultural systems is driving climate change, environmental degradation and biodiversity loss (Rey Benayas and Bullock, 2012). To maintain high yields, these cropping systems require significant inputs of energy (Zhou et al., 2021), water (Rosa et al., 2020), fertilizers (Nguyen et al., 2024) and plant protection products (Maggi et al., 2019). Global food supplies increased thanks to agricultural expansion and intensification, which, however, caused detrimental effects to the environment and the interconnected ecosystems (Foley et al., 2005; Rey Benayas and Bullock, 2012). LULC variations are one of the non-climatic hazards responsible for changes in terrestrial and freshwater ecosystems (Pörtner et al., 2021). According to Birk et al., (2020), the impacts on ecosystems due to LULC variations currently predominate on the impacts due to climate change, but greater interactive effects of non-climate and climate hazards are now occurring. In recent years, biodiversity studies focused on greenhouse systems have started to emerge. Castro et al. (2019) document the challenges in conciliating greenhouse horticulture with the unique habitats present in the hotspot of Mediterranean greenhouses in the Spanish drylands. Messelink et al. (2021) study plant diversity inside and outside greenhouses to evaluate their contribution to pest control. Finally, Zhou et al. (2021) analyse to which extent four greenhouse systems for producing tomatoes are able to meet pertinent Sustainability Development Goals adopted by the United Nations. The opportunity to include protected agriculture in LULC change studies can thus lead to a more comprehensive picture of the factors affecting natural resources.

The Food and Agriculture Organization of the United Nations (FAO) reports about 33% of land being used for farming globally (or 4.7 million km^2) (FAO, 2022). Therefore, LULC mapping and monitoring holds significant relevance and warrants thorough analysis (Campos et al., 2024). Satellite remote sensing products play a pivotal role in global near real-time agricultural LULC classification. These satellite products supply key information to manage agricultural areas for food security and to drive policy-making for environmental sustainability (Defourny et al., 2019). Numerous studies within the scientific literature delve into these topics (Sishodia et al., 2020; Wójtowicz et al., 2016; Steven and Clark, 2013), consistently amplifying the growing significance and interplay between remote sensing and agriculture (Khanal et al., 2020). Operational satellite-based agriculture monitoring at global scale is advancing quickly (Defourny et al., 2019; Weiss et al., 2020), but greenhouse horticulture mapping is not accounted for in such applications, as in Tsendbazar et al. (2021) and Brown et al. (2022).

Available studies developed methods to recognize plastic greenhouses using a plethora of approaches and satellite missions, which are summarized in la Cecilia et al. (2023a), and highlighted the presence of plastic greenhouses districts located inside and outside Europe. For instance, European districts are reported to be in the Almería region in Spain (Aguilar et al., 2015), the Anamur district in Turkey (Balcik et al., 2020), the surroundings of Marina di Acate in Italy as well as the Ierapetra district in Greece (la Cecilia et al., 2023a) and in The Netherlands (Dekker, 2003 and la Cecilia et al., 2023a). Globally, other major clusters of greenhouse cultivation are found in China (Ma et al., 2021), Morocco (Simou et al., 2023), and Mexico (Perilla and Mas, 2019). The Chinese territory has seen a proliferation of greenhouses and an array of studies addresses their classification using various types of remote sensing data (Wang et al., 2023; Ou et al., 2021). An important and recent study that accomplished to map permanent high-tunnels, comprising a group of plastic greenhouses, worldwide is by Tong et al. (2024a). The authors used very high-resolution commercial satellite images to identify high-tunnels using a Convolutional Neural Network (CNN). The authors report a total of 13 227 km^2 of greenhouses, with 65 greenhouse districts larger than 15 km^2.

The sprawling of greenhouse horticulture districts (Briassoulis et al., 2016; Espí et al., 2006), the presence of other forms of protected agriculture (e.g., low-tunnels and plastic mulch) and their variability over time motivate the need for having a methodology for regional scale mapping that goes beyond current limitations being specific for areas, times, requiring high computational times or commercial data. In this study, we developed a pan-European map of the presence of protected agriculture over agricultural soils, as reported in the CORINE Land Cover 2018 dataset (reference in the bibliography). For developing such product, we integrated the random forest-based pixel-level Open field and Protected Agriculture land cover Classifier (OPAC) developed using Sentinel-2 L2A data (la Cecilia et al., 2023a) in the Google Earth Engine platform (GEE; https://earthengine.google.com/)). GEE provided the storage

and computational power needed not only to achieve continental-scale and continuous mapping but also to introduce several masks (single or time-composite products from multiple data sources) for reducing misclassifications. The output product, derived from freely available satellite imagery in conjunction with open-source platforms, can be harnessed to estimate the overall extent of protected agriculture across the European continent periodically. Such insights are invaluable for the evidence-based development and implementation of European and regional policies aiming to make informed decisions on land management and resources management.

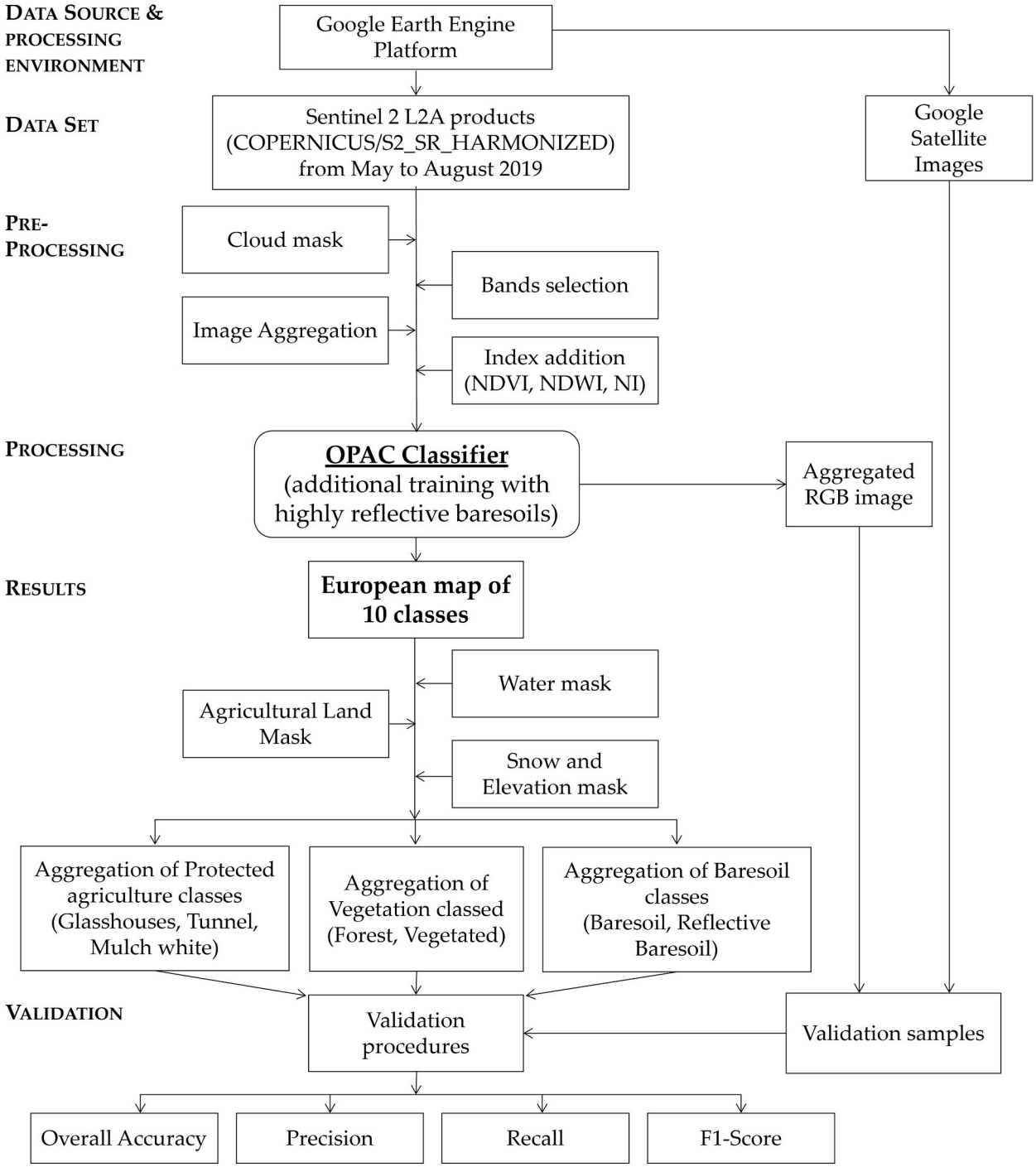

Fig. 1. Workflow to generate the 10-classes land cover map and its aggregation into the validated 6-classes land cover map.

2. Methods and datasets

The Protected Agriculture product is developed in this research by running an improved version of OPAC (la Cecilia et al., 2023a) in the GEE cloud computing platform (Gorelick et al., 2017). We implement additional methods and datasets (single or time-composite products from multiple data sources all provided within the GEE platform) for reducing known misclassification issues. The basis for classification in this study relies on atmospherically corrected Sentinel-2 images (L2A). These Sentinel images form the cornerstone for classification, offering a wealth of spectral information that aids in distinguishing various land cover types. The twin platform of Sentinel-2 A and B provides a range of bands, including four at 10-m spatial resolution, six at a 20-m resolution, and three at a 60-m resolution. These bands cover a wide spectral range from 440 nm to 2.2 μm and feature a radiometric resolution of 12 bits. The use of this sensor is well-established in the fields of agriculture but also for greenhouse classification (Segarra et al., 2020; Zhang et al., 2022; Ibrahim and Gobin, 2021).

The product can be developed at any time Sentinel-2 L2A images are available. Here, we used Sentinel-2 L2A images relative to the year 2019 for two reasons. First, the year is close to 2018, which corresponded to the latest update of the CORINE Land Cover 2018 (reference in the bibliography) map, which we use in the workflow. Second, it allows for qualitatively comparing our pan-European map of protected agriculture with the only alternative one recently published by Tong et al. (2024a,b).

2.1. Workflow to generate the land cover map

The workflow to generate the land cover map described in the following paragraphs and it is shown in Fig. 1.

Description of the random forest-based classifier. OPAC training is detailed in la Cecilia et al. (2023a). Briefly, OPAC is a random forest-based, nine-class (listed in Table 1), single Sentinel-2 L2A product, pixel-level classifier. It had been trained on 5151 manually selected pixels at, or resampled to, 20 m resolution sampled from forty Sentinel-2 products. Each pixel is a 13-dimensional feature vector composed by ten Sentinel-2 L2A spectral bands (i.e, Bands B1, B2, B3, B4, B5, B6, B7, B8, B11, B12 with central wavelengths at 442.7, 492.4, 559.8, 664.6, 704.1, 740.5, 782.8, 832.8, 1613.7, 2202.4 nm) and three spectral indices, which are the Normalized Difference Vegetation Index (NDVI = [B8-B4]/[B8+B4]) by Rouse et al. (1974), the Normalized Water Moisture Index (NDWI = [B8-B11]/[B8+B11]) by Gao (1996) and a normalization index for plastic greenhouses (NI = [2 × B8-B4-B12]/[2 × B8+B4+B12]) by Zhang et al. (2022).

Improvement of the random forest-based classifier. In this research, we used an improved version of OPAC, which was deemed necessary after large areas in Turkey and Spain, where the top-soil was rich in carbonate calcium (Batjes, 2016; Calero et al., 2018; Gallagher and Breecker, 2020; Santos-Francés et al., 2022 as well as personal communication from Benjamin Mary and Miguel Ángel Herrezuelo Bermúdez), were affected by misclassification issues. The improvement consisted in training OPAC with additional randomly selected 300 pixels of highly reflective bare soils from Turkey, which were previously misclassified as protected agriculture (e.g., any class listed in Table 1 among “Mulch_white”, “Tunnel” and “Glasshouse”). Three hundred pixels were chosen to maintain a class-balanced classifier. These 300 pixels constituted a new class called “Reflective baresoil”. The final training dataset is freely available at the link provided in the Data Availability Statement.

Integration of the random forest-based classifier in the Google Earth Engine platform. The significant methodological innovation of this study is the integration of OPAC in the GEE platform. To do this, we imported the training set in the GEE platform and trained the random forest model with the same parametrization as OPAC, that is:

- two features randomly sampled as candidates at each split;

Table 1
OPAC’s classes as described in la Cecilia et al. (2023a) and the new class called “Reflective_baresoil”. All classifications are retained for any confidence estimate.

Class label	Description	Domain/Land System Group	Rationale
“Mulch_white”	White plastic mulch and white soil cover sheets.	Agricultural	Represents areas where reflective plastic sheets are used to improve soil moisture and weed control.
“Tunnel”	White low- and high-greenhouses in plastic.	Agricultural	Indicates structures for controlled crop growth, reflecting a high-intensity agricultural system.
“Glasshouse”	High-tech greenhouses, typically made from glass or polycarbonate.	Agricultural	Identifies advanced agricultural setups for high-value crops or specialized cultivation.
“Vegetated”	Areas covered with low vegetation (crops, meadows, etc.) and tall vegetation (orchards).	Agricultural and Natural	Represents multifunctional vegetated land used for both natural and agricultural purposes.
“Forest”	Areas covered with forests.	Natural	Distinguishes forested ecosystems
“Baresoil”	Soil that is bare.	Transitional or Natural	Identifies areas undergoing land-use change or with none or minimal vegetative cover.
“Reflective baresoil”	Reflective bare soil, likely rich in calcium carbonate.	Natural	Represents soils with a high albedo, reflecting a significant amount of solar radiation.
“Water”	Ponds, lakes, streams and rivers.	Natural	Represents water bodies.
“Snow”	Snow.	Natural	Captures seasonal or permanent snow cover.
"Shadow”	Cloud and tree shadows.	Other	Identifies shaded areas that may obscure underlying land cover features.

- two-hundred decision trees to grow;
- one as the minimum size of the terminal node.

OPAC always returned a label for each classified pixel, that is, we did not use any confidence estimate to either accept or disregard the output.

There exist known classification limitations resulting from clouds and land cover spectral ambiguities. To reduce false positives of pixels with protected agriculture, we exploited the power of the GEE platform, which allowed for synthesizing time dependent variables and using auxiliary datasets.

Sentinel-2 dataset. In the GEE environment, we used the COPERNICUS/S2_SR_HARMONIZED dataset as the source of Sentinel-2 data.

Time period. We selected the late spring and early summer period being the time window with the greatest likelihood to have protected agriculture (May to August in the Northern hemisphere).

Cloud mask. For the selected period, we created the image collection by retaining only cloud free pixels according to the novel Cloud Score + algorithm (Pasquarella et al., 2023) using a threshold of 0.6. Contrary to other cloud masks, the Cloud Score + algorithm is effective at distinguishing between greenhouses and clouds.

Image aggregation. To further limit the possibility of temporary highly-reflective pixels and to preserve the coherent information of each pixel, among the whole collection, we extracted per each pixel the spectra with the minimum value in the green band (560 nm). The aggregated image was fed to OPAC for land cover classification.

Water mask. In the GEE platform, it is available the MOD44W V6 land/water product at 250 m resolution derived from the Moderate Resolution Imaging Spectroradiometer (MODIS) for the whole globe. We used this product to mask out ocean and sea water pixels. The product includes seas and oceans and inland waters relative to the year 2015, which was the last year before discontinuation of the product (Carroll et al., 2017).

Snow and elevation mask. Highly reflective plastic roofs can be misclassified as snowy pixels. For the aggregated image to classify, we computed the Normalized Difference Snow Index, defined as NDSI=(B3-B11)/(B3+B11), and we joined the corresponding altitude according to the United States Geological Survey (USGS) Shuttle Radar Topography Mission digital elevation data (DEM), version 3, product available at a spatial resolution of about 30 m (Farr et al., 2007). Eventually, we reclassified as "snow" those pixels with an elevation >1000 m and a NDSI >0.3. The reclassification excludes "water" pixels that meet the conditions regarding elevation and NDSI. This is because we identified some "water" pixels above 1000 m with a NDSI >0.3, which would be erroneously reclassified as "snow".

Agriculture land mask. In some cases, given the spatial and spectral resolutions of Sentinel-2, the mixed pixel problem could lead to misclassifications. Typical examples are roads and buildings adjacent to vegetation, some kind of roofs and ephemeral streams with a high reflective stream bed covered by patchy low vegetation (case studies already tested in la Cecilia et al., 2023a). To mitigate these false positives, we applied the CORINE Land Cover 2018 (reference in the bibliography), or CORINE for brevity, as a mask to retain only agricultural fields (CORINE identifiers from 211 to 244) located in Europe. We tested other global maps as masks including the "Dynamic World" by Brown et al. (2022), the "ESA WorldCover 10m v100" by Zanaga et al., (2021) and the "Global map of Local Climate Zones" by Demuzere et al. (2022). However, these maps classify protected agriculture as urbanized areas (i.e., "impervious" or "built-up" land covers).

Reclassification. OPAC cannot well separate between "vegetated" and "forest", and therefore, these two classes were grouped together simply as "vegetated". Similarly, the three classes of protected agriculture (i.e., "Glasshouse", "Mulch_white" and "Tunnel")

Table 2
CORINE data subdivision for validation purposes. [(1)]M49 geographic areas prepared by the Statistics Division of the United Nations Secretariat for statistical uses (https://unstats.un.org/unsd/methodology/m49/). [(2)]Observed climate zones in Europe prepared by the European Environmental Agency (https://www.eea.europa.eu/ds_resolveuid/4a39a05230994509b716ad983e931278).

Countries/States	ID subarea	Geographic Area[(1)]	Predominant climate zones 1996–2016[(2)]
France	1	Western Europe	Mediterranean, Maritime North
Italy	2	Southern Europe	Mediterranean, Maritime South, Boreal South
Switzerland	3	Western Europe	Boreal South, Continental
United Kingdom	4	Northern Europe	Maritime North, Continental
Iceland	5	Northern Europe	No data
Slovakia, Czechia, Poland	6	Eastern Europe	Continental, Pannonian
Lithuania, Latvia, Estonia	6	Northern Europe	Continental, Nemoral
Portugal, Spain	7	Southern Europe	Mediterranean, Maritime South, Maritime North
Greece	8	Southern Europe	Mediterranean
Turkey	8	Western Asia	Mediterranean, Maritime South, Pannonian, Continental, Nemoral
Germany, Netherlands, Belgium, Luxemburg	9	Western Europe	Maritime North, Continental, Pannonian
Denmark, Norway, Sweden, Finland	10	Northern Europe	Continental, Nemoral, Boreal South, Boreal North
Austria	11	Western Europe	Continental, Pannonian, Boreal South
Hungary, Romania, Bulgaria	11	Eastern Europe	Pannonian, Nemoral
Slovenia, Croatia, Serbia, Albania, Montenegro, Kosovo*, North Macedonia	11	Southern Europe	Mediterranean, Pannonian, Continental

did not separate well, and therefore, were grouped together and called "protected agriculture".

2.2. Validation

To the best of our knowledge, it does not exist a curated, temporally- and spatially-sparse validation set for protected agriculture. OPAC was initially trained and validated using 5151 pixels from Switzerland and Spain (la Cecilia et al., 2023a,b). Here, we briefly describe the procedure followed to compile one validation set for the produced European map. We divided the CORINE extent into eleven subareas to remain within the allowed memory limit by the GEE platform. The eleven identified areas are listed in Table 2. For each of the chosen areas, we manually selected at least 30 pixels in a balanced manner, that is, 10 for each of the classes "protected agriculture", "vegetated" and "baresoil". Our interest was to identify a minimum number of locations, which were, when possible, far away from each other to encompass the climatic and geographic variability per country and at the European level. Not only these three classes were the more interesting ones for our purpose, but also (1) the CloudScore mask removes shadows (which is one class), (2) the CORINE map masks out many water bodies and (3) snow was not found in all countries in the studied period. Where possible, we selected a maximum of 30 pixels per country, but in few northern countries, we could not find enough greenhouse tunnels. In total, we labelled 450 pixels based on our interpretation of the aggregated RGB image and the very-high resolution, but asynchronous, Google Satellite image available in the GEE platform (Fig. 1). We then extracted the land cover classification of the validation set by OPAC. Finally, we calculated the classification performance scores using EQ (1) to EQ (4), where *TP* is the number of true positives, *TN* the number of true negatives, *FP* the number of false positives and *FN* the number of false negatives:

$$Overall\ accuracy = \frac{(TP + TN)}{(TP + TN + FP + FN)} \quad \text{EQ 1}$$

$$Precision = \frac{TP}{(TP + FP)} \quad \text{EQ 2}$$

$$Recall = \frac{TP}{(TP + FN)} \quad \text{EQ 3}$$

$$F1\text{-}score = 2 \times \frac{Precision \times Recall}{(Precision + Recall)} \quad \text{EQ 4}$$

The analysis of the quantitative performance scores was then complemented with a visual assessment of the classification model performance to qualitatively show the robustness of the model over tens of thousands of pixels.

3. Results

We present the results relative to the year 2019 for the reasons explained in Section 2.

3.1. Classification performance scores

The overall accuracy calculated using EQ (1) for the class "protected agriculture" was 94%, for "vegetated" was 96% and for "baresoil" was 97% (Table 3). The precision calculated with EQ (2) was high for "protected agriculture" (1.00) and it indicated the lack of false positives. Though, the visual inspection of the output map showed that land covers including mining areas, reflective roofs, ephemeral streams and sandy soils, which were still encompassed within the agricultural areas of the CORINE map, could be misclassified as "protected agriculture". Therefore, it is likely that precision would decrease should highly-reflective surfaces be present in the validation set. The precision for the other two classes decreases to a mean value of 0.91 because sparse and low vegetation could be interpreted as "vegetated" but classified as "baresoil" and vice versa. The recall score calculated with EQ (3) for "protected agriculture" was 0.83 and implied the presence of false negatives. These false negatives are plastic tunnels with reflectance values in the aerosol band at 443 nm lower than 0.1 and they look light gray. Indeed, OPAC was trained with reflectance values in B1 > 0.1 to neglect forests-formed aerosols leading to the formation of the blue haze (Zhang et al., 2009). The F1-score calculated with EQ (4) is defined as the harmonic mean of the precision and recall scores. It is a recommended score in case the classes in the dataset are imbalanced. Because we appropriately compiled a balanced validation set, we report the F1-score mainly for comparability across studies employing different classification models. The classes "vegetated" and "baresoil" stood out with a F1-score of 0.94 and 0.95, respectively, reflecting that the model had few false positives and false negatives in the compiled validation set. The class "Protected

Table 3
Tabulated classification performance scores calculated with EQ (1) to EQ (4).

Class	Overall accuracy (%)	Precision	Recall	F1-score
Protected agriculture	94	1.00	0.83	0.91
Vegetated	96	0.89	1.00	0.94
Baresoil	97	0.93	0.97	0.95

agriculture" showed a slightly lower F1-score of 0.83, still striking a good balance between precision and recall. The obtained F1-score results align well with results from other researchers tackling the classification of plastic greenhouse using satellite imagery (Yang and Huang, 2024; Ou et al., 2021).

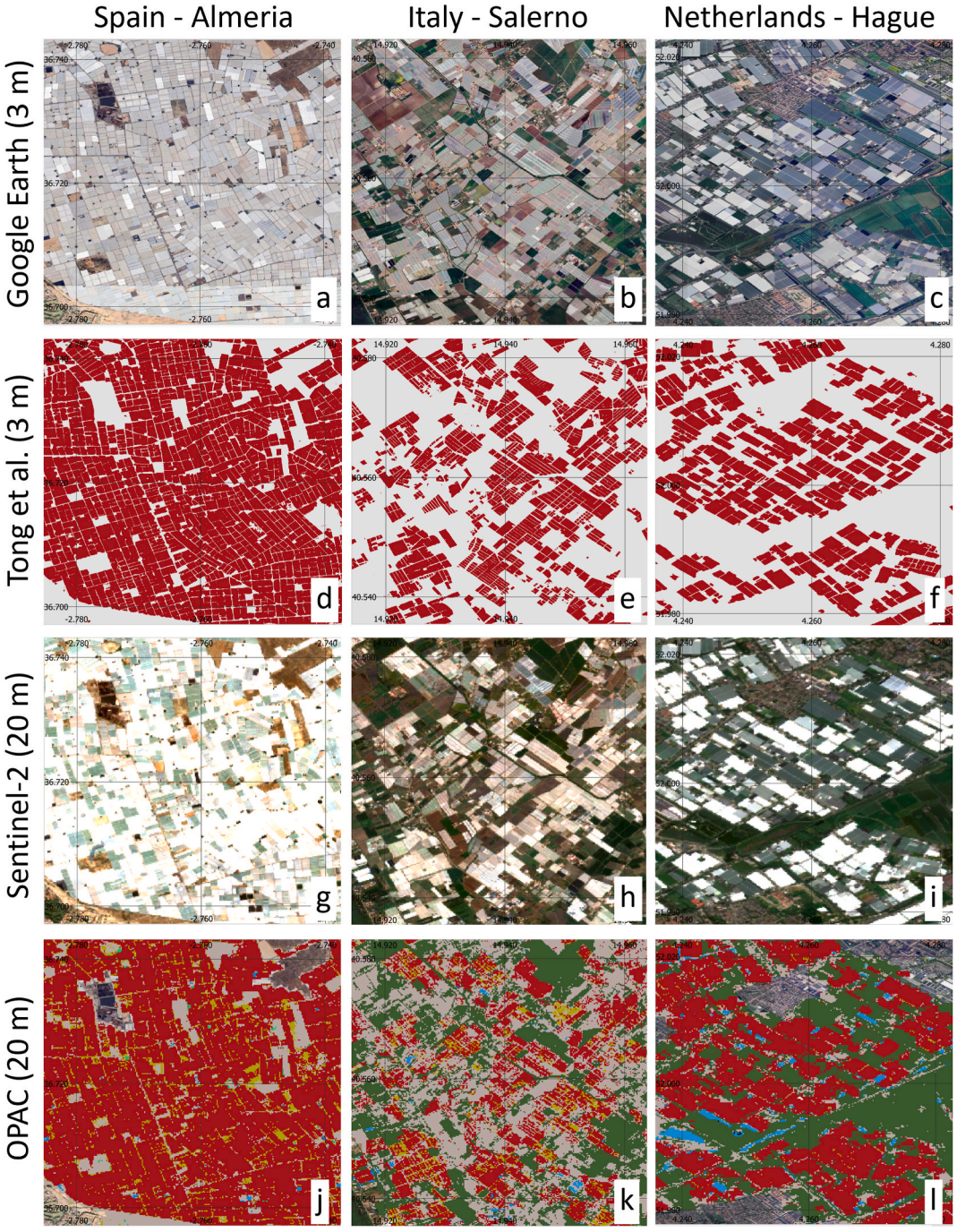

Fig. 2. Zoomed in visualization of the classification output. Panels in the first row depict Google Earth true color images (TCI) at <3 m pixel resolution; second row, classification output by Tong et al. (2024b) (red is "greenhouse" and gray is "other"). Left and centre panels for Spain and Italy, respectively, where plastic greenhouses are present. Right panels for The Netherlands where glass greenhouses are present; third row, Sentinel-2 TCI (aggregated image from May to August) at 20 m; last row, classification output using OPAC at 20 m masked by CORINE (reference in the bibliography) (red is "protected agriculture", green is "vegetated", gray is "baresoil", light blue is "water", olive is "reflective soil").

3.2. Visual assessment of the classification model

The visual assessment of the classification model performance complements the quantitative analysis carried out in Section 3.1 and it qualitatively shows the robustness of the model over tens of thousands of pixels. The comparison between high resolution true color images (TCI) from Google Earth (first row in Fig. 2) and Sentinel-2 (third row in Fig. 2) revealed that the presence of greenhouse, both in plastic and in glass, were stable since 2019 (year of the processed Sentinel-2 images until the images in Google were taken). These areas are notoriously known for their historical importance as greenhouse horticulture districts. OPAC was able to identify greenhouses both in plastic typical of Mediterranean areas (e.g., analysed areas in the south of Spain and Italy depicted in Fig. 2j and k) and in glass found in colder climates (e.g., studied area in The Netherland shown in Fig. 2l). Few pixels of the plastic greenhouses were misclassified as "reflective baresoil". This highlighted the tradeoff between the identified necessity to distinguish between greenhouses and reflective soils in the rural areas of Spain and Turkey. Also, few plastic greenhouses were classified as bare soil in the area in Italy (Fig. 2k). As presented in Section 3.1, these greenhouses very likely have a reflectance lower than 0.1 in the aerosol band at 443 nm of Sentinel-2, hence, they could not be classified as protected agriculture by OPAC. The results obtained using OPAC, which classifies Sentinel-2 images with a random forest model, were consistent with those produced by Tong et al. (2024a,b), which classified PlanetScope imagery using a convolutional neural network and extracted single greenhouses only when the distance between two objects was greater than 10 m (Fig. 2d–f).

3.3. Protected agriculture mapping

OPAC mapped protected agriculture everywhere in the pan-European research area (Fig. 3). The densest areas were found in the south mostly, although some dense areas appeared in the centre of Europe. Very sparse protected agriculture was mapped in the most northern countries.

In Southern Europe, the densest areas of protected agriculture matched well with the areas historically known from location-specific studies, such as the Almeria region in Spain. OPAC identified very important greenhouse districts in the south and north of Italy (e.g., in the regions of Campania, Puglia, Sicilia and Lazio as well as in Lombardia and Veneto). OPAC mapped few dense areas of protected agriculture in Albania. Regarding Turkey, long stretches of coastal areas were covered by plastic greenhouses. However, in the centre of the country, widespread areas were classified as protected agriculture within the agriculture land cover of CORINE, whereas the very high resolution images depicted a top layer of clay-like material above the soil among orchards. The same was true also for some areas in the centre of Spain.

OPAC mapped dense areas of protected agriculture in the centre of Europe. This was consistent with traditional knowledge on the global importance of the greenhouse horticultural industry in The Netherlands. At these latitudes, the climatic conditions are less favourable to the presence of Mediterranean plastic greenhouses, rather they require the construction of glasshouses. The locations of greenhouse districts by Tong et al. (2024b) and those of dense areas by OPAC agreed. OPAC mapped a significant higher number of dense areas in Germany and Poland. However, the visual inspection revealed that many pixels classified as protected agriculture were

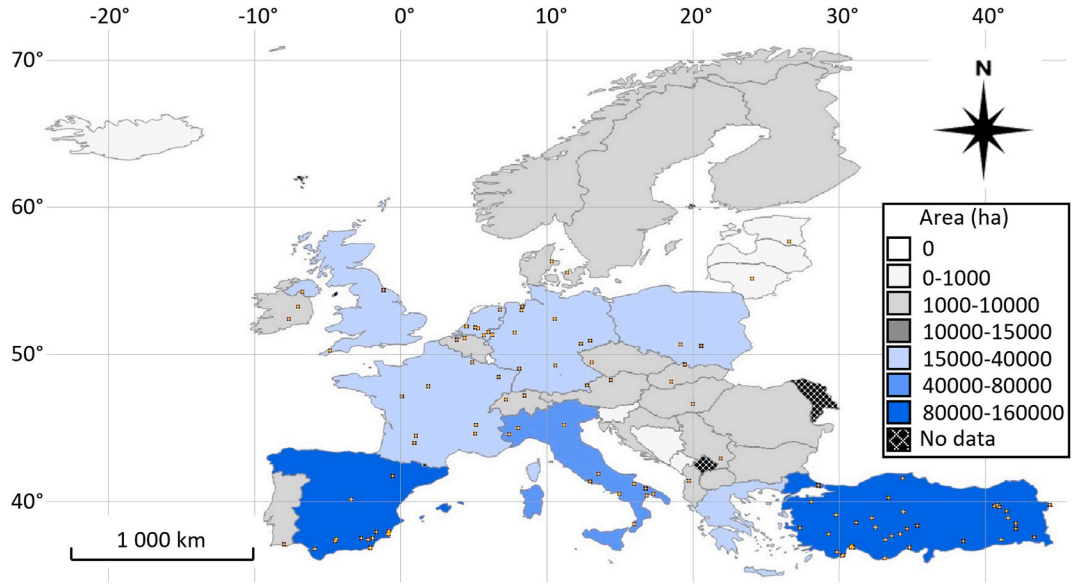

Fig. 3. Background color by state depicts the total area in hectares mapped by OPAC by state in 2019, cropped on the CORINE (reference in the bibliography) agricultural area. Yellow-colored buffered-pixels for visualization purposes indicate the location of the densest areas of protected agriculture according to OPAC. Country-level boundaries from the FAO Global Administrative Unit Layers of 2015 (FAO, 2015). Coordinates in EPSG: 4326.

white roofs of farmyards, which may serve the purpose of improving the welfare of livestock (Santunione et al., 2017).

3.4. Protected agriculture extension

The total area of protected agriculture mapped by OPAC achieved 5300 km^2. The largest areas of protected agriculture were found in Turkey with about 1600 km^2, in Spain with 1240 km^2 and in Italy with 630 km^2 (Fig. 4a). Protected agriculture in Germany and France exceeded 230 km^2, in Poland, The Netherlands and United Kingdom exceeded 150 km^2, in Greece almost achieved 140 km^2 and in Portugal almost achieved 80 km^2.

The Mediterranean islands of Malta use almost 1.0 % of the total agricultural area for protected agriculture (Fig. 4b). After Turkey and Spain with more than 0.3 % of agricultural area covered by protected agriculture, The Netherlands achieved 0.50 %, which was larger than the percentage for Italy of about 0.3 %.

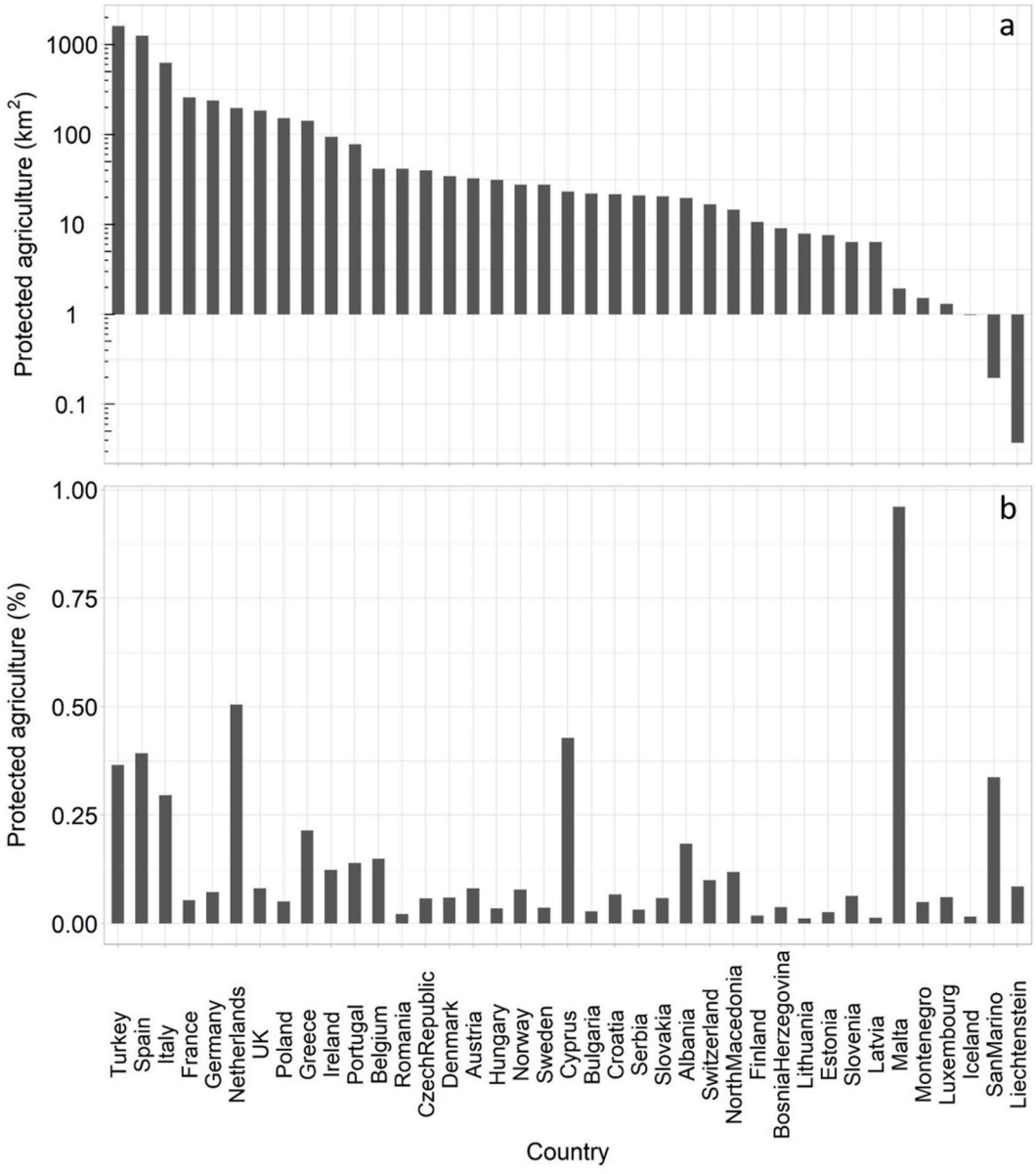

Fig. 4. Country-specific quantitative analysis on (a) the extension of protected agriculture in km^2, note the y-axis in log10 scale, and (b) the percentage of protected agriculture with respect to the CORINE (reference in the bibliography) agricultural area.

3.5. Generalization of OPAC beyond the pan-European level

Given the overall robust capabilities of OPAC to classify agricultural areas at the pan-European level, we verified the possibility to identify protected agriculture at few major greenhouse districts mapped by Tong et al. (2024a). The selected areas regarded very different geographical contexts spanning among China, Morocco and Mexico. The comparison between more recent Google Earth

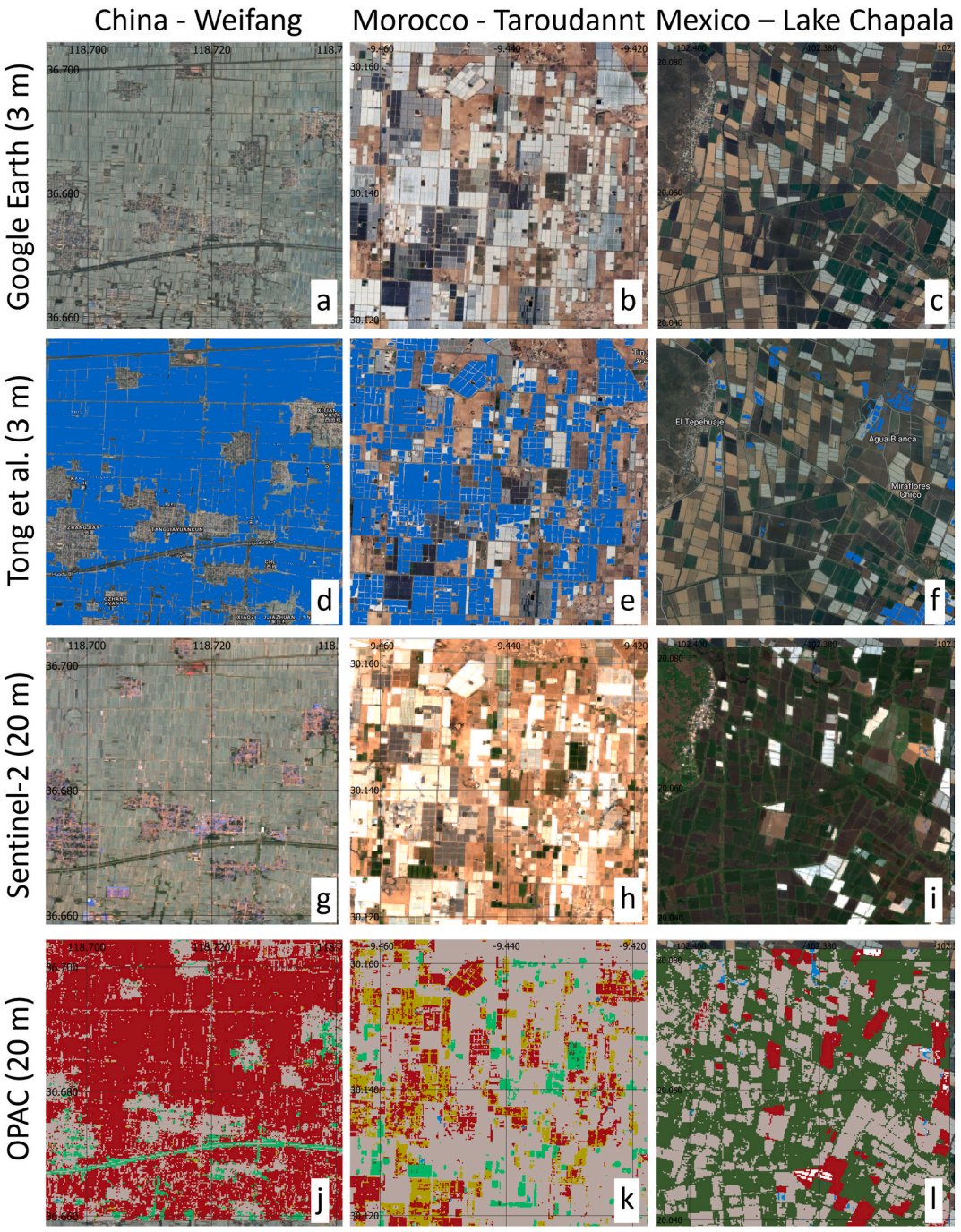

Fig. 5. Zoomed in visualization of the classification output. Panels in the first row depict Google Earth true color images (TCI) at <3 m pixel resolution; second row, classification output by Tong et al. (2024b) (blue is "greenhouse" and transparent is "other"). Left, centre and right panels for China, Morocco and Mexico, respectively, where plastic greenhouses are present; third row, Sentinel-2 TCI (aggregated image from May to August) at 20 m; last row, classification output using OPAC at 20 m masked by CORINE (reference in the bibliography) (red is "protected agriculture", green is "vegetated", gray is "baresoil", light blue is "water", olive is "reflective soil").

images and older Sentinel-2 images revealed the presence of a growing number of greenhouses, or at different locations, in Morocco and Mexico (first and third rows and last two columns, respectively, of Fig. 5). This finding would point to the necessity to update the product of the locations of greenhouses at least annually. In China, OPAC correctly identified the large area covered by plastic greenhouse and classified the majority of urban areas as bare soil, except in few cases (Fig. 5j). In Morocco, about 30% of plastic greenhouses were misclassified as "reflective baresoil" (Fig. 5k), which was again the tradeoff paid in order to reduce the area of reflective soils classified as protected agriculture in rural Spain and rural Turkey. In Mexico, OPAC correctly classified the variety of land covers. Only two greenhouses in the north and south of the studied area were confused with snow (white pixels). OPAC also mapped bending lines of "water" pixels in the area, which were possibly caused by previous flooding in the area. In general, the classifier by Tong et al. (2024a) mapped all the greenhouses in China (Fig. 5d). As far as the areas in Morocco and Mexico are concerned, it appeared that the classifier mapped all the greenhouses (Fig. 5e and f) captured in the Sentinel-2 images relative to 2019 (Fig. 5h and i). Thus, the unidentified plastic greenhouses shown in the background were built at a later stage.

4. Discussion

In the following section, we highlight the strengths of the proposed framework. Then, we evaluate opportunities to supersede its limitations and how the identified solutions would allow for operational global mapping of protected agriculture. Finally, we discuss the impacts of protected agriculture on the environment.

4.1. Strengths of the framework

The major advantages of the developed workflow regard the classification speed of large areas with the frequent revisit period, thus allowing for regularly updating maps of protected agriculture across Europe. Further, the possibility to exploit the multispectral capabilities of freely available Sentinel-2 data enables to robustly classify other land covers other than protected agriculture. In this sense, the framework advances those studies focusing on plastic greenhouse mapping by integrating the discipline with the concurrent classification of other LULC typical of agricultural areas. The leveraged freely available global datasets allow for widespread accessibility. The study demonstrates commendable overall accuracy, particularly in classifying the three selected classes for model validation: we obtained an accuracy of 94% for "protected agriculture", 96% for "vegetated" and 97% for "baresoils". These results align with the relevant scientific literature and, in some cases, even exhibit slightly superior performance. Comparable studies (Jiménez-Lao et al., 2020), albeit focusing on small-scale plastic greenhouse-covered study areas, report accuracy values ranging from 88% to 92% when working with QuickBird and Ikonos images (Agüera et al., 2006, 2008), up to 94% with very high-resolution Worldview2 imagery using the Random Forest algorithm (Koc-San, 2013), and up to 95% when employing Landsat 8 images and a Support Vector Machine classifier (Lanorte et al., 2017). Nonetheless, we highlight that those studies were not tested at other locations, whereas the new framework showed a robust scalability even at locations away from the training areas.

The modular integration of masks based on remote sensing indices (i.e., the NDSI) and informative layers (i.e., cloud, water, elevation and agriculture) minimizes classification errors as well as enables users to use location-specific ancillary information. This last feature was important because more accurate local data would further reduce the number of misclassified pixels. For example, misclassified pixels can still occur within the CORINE agriculture layer for some land covers, as it is discussed in the next section 4.2. Still, the availability of parcel level data effectively removed the majority of those cases (as shown in la Cecilia et al., 2023a).

4.2. Limitations of OPAC and solutions for improvement

The current framework happened to overestimate the extension of protected agriculture in the presence of reflective land covers. Regarding agricultural uses largely affected by the misclassification issue, we highlight the case of Turkey and Spain, where orchards grow above reflective terrains. In fact, the signature of greenhouses measured by Sentinel-2 corresponded to a vegetated area with reflectance values at all bands shifted upward (la Cecilia et al., 2023a). Thus, the mixed presence of vegetation and reflective background in a pixel would be mistaken for a greenhouse. The reflective terrains in Turkey and Spain are indeed rich in carbonate calcium (Batjes, 2016; Calero et al., 2018; Gallagher and Breecker, 2020; Santos-Francés et al., 2022 as well as personal communication from Benjamin Mary and Miguel Ángel Herrezuelo Bermúdez). Carbonate calcium is also the same material used to shade Mediterranean-like plastic greenhouses in summer. OPAC was trained to classify white-panted Mediterranean greenhouses, for which the multi-spectral signature revealed high reflectance across all bands and the loss of the peculiar signature of vegetation (la Cecilia et al., 2023a). In this study, for expanding the worldwide applicability of OPAC, we introduced a new class to distinguish highly reflective bare soils. In doing so, we faced a trade-off between the necessity to better distinguish between greenhouses and reflective soils in the rural areas of Spain and Turkey, without losing the capability to map plastic greenhouses elsewhere (i.e., in Morocco). One solution to solve the misclassification problem would be to acquire high spatial resolution TCI data and run a trained CNN model (Tong et al., 2024a) to ascertain the presence of greenhouses. In order to avoid incurring on prohibitive costs, commercial space agencies would need to develop licenses at reasonable prices for education and research institutions (as some industries are actually already doing). Alternatively, an efficient solution concerns to add to the multi-spectral capability of public multi-spectral satellites two bands at 1644 nm and 1729 nm (Zhou et al., 2022; Parmeggiani et al., 2024) for the accurate detection of plastic covers. Indeed, these authors have demonstrated that plastic materials exhibit distinctive spectral peaks at specific wavelengths. Sentinel-2 lacks these plastic-sensitive bands, and therefore, there exists a technological limitation for accurately detecting plastic greenhouses. Incorporating such dedicated spectral bands would enable robust and rapid global monitoring of plastic-covered greenhouses with an

expeditive normalized index (Parmeggiani et al., 2024) in alternative to deep learning models (Zhou et al., 2022).

Other land uses, contaminating the CORINE agriculture layer, and causing false positives for the class "protected agriculture", were highly reflective land covers, such as ephemeral streams, certain types of roofs, mining areas, among other reflective anthropic surfaces. However, we decided not to manually remove these areas to highlight the challenges of classification and to maintain the automatic methodology without user intervention. There may happen false negatives for the class of protected agriculture. These false negatives were plastic tunnels with reflectance values in the aerosol band at 443 nm lower than 0.1 and they looked light gray. OPAC was trained with reflectance values in B1 $>$ 0.1 to neglect forests-formed aerosols leading to the formation of the blue haze (Zhang et al., 2009). Further research to disentangle these two land covers will improve OPAC's classification accuracy. Finally, a time-series analysis-based approach was suggested to identify plastic-mulched farmlands, and thus, reduce the confusion with other classes of protected agriculture (de Souza et al., 2024). While this should undergo extensive testing, it could be easily implemented in the workflow should there be need to distinguish between the classes of protected agriculture.

4.3. Applicability of OPAC without agricultural masks

OPAC potentially allows for mapping protected agriculture at the global scale, thus creating relevant information especially in countries with a significant presence of greenhouses, such as Mexico, China, and Morocco (Perilla and Mas, 2019; Ou et al., 2019; Acharki et al., 2023). We expected that the misclassification issues discussed in Section 4.2 were exacerbated in CORINE land uses other than those limited to agriculture, such as in urban and industrial areas. An encouraging finding when applying OPAC outside Europe (Mexico, China and Morocco), not constrained on agricultural areas, was the qualitative observation that urban areas were classified as bare soils. However, we had to recognize that those selected areas lacked reflective land covers, such as technological cool roofs, or carbonate-rich topsoils. To achieve a robust assessment of the global map of protected agriculture developed with the presented framework, we could envisage a collaborative international effort to run and validate OPAC country-by-country. For a more autonomous process, we are confident that expanding the multi-spectral capability of current public satellite missions to measure in the plastic-specific reflectance bands (Section 4.2) will improve the mapping accuracy of protected agriculture. While this further work appears to require a tremendous effort, the global map can reveal critical hotspots of agricultural technological development contributing to global food trades. These hotspots are expected to require expert knowledge to comprehensively inform policy makers for good governance in the long-term.

4.4. Hotspots of altered environmental processes

Sentinel-2 and OPAC allow for monitoring the land cover of agricultural areas, with the unique inclusion of protected agriculture. This will improve the realism of environmental modelling and satellite-based monitoring in hotspots of protected agriculture. In the latter case, new techniques for generating planetary variables (e.g., soil moisture and irrigation), with satellite data (Modanesi et al., 2021) would not work below the cover of greenhouses. Here, we discuss the implications of greenhouse horticulture on water resources management, which may depend on local climate variables and traditional values. It has been demonstrated that greenhouse systems reduce the daily ET (Fernández et al., 2010; la Cecilia et al., 2024; Locatelli et al., 2024). This has significant implications since ET is typically one major component of the hydrological budget (Ryken at el., 2022), with its signature notable even in surface- and groundwater dynamics (la Cecilia and Camporese, 2022). Rainfall is often considered the other major component of the hydrological budget (Ryken et al., 2022). In protected agriculture in water scarce areas, rainfall is generally retained in irrigation basins. This would cause a reduction in runoff or infiltration, as well as a lower pressure on other sources, such as groundwater or abstracted surface water. Yet, while semi-arid places offer a favourable climatic situation for greenhouse horticulture, they inherently suffer from the paucity of water. Garcia-Caparros et al. (2017) and Castro et al. (2019), while analysing in depth common practices in the hotspot of Almeria (Spain), they identified the excessive overexploitation of groundwater for irrigation due to the lack of other water sources. The authors continued by explaining the solutions continuously searched for by water managers to help farmers supplying the necessary water to crops. Novel additional water sources, generally not yet accounted for in hydrological modeling, included desalinated seawater and reclaimed wastewater. Thus, water managers converted outlets into inlets. Garcia-Caparros et al. (2017) present also a particular land management practice that helps to save water. In Almeria, farmers rely on cascade cropping, whereby the leachate from the previous crop is collected in the sub-surface drainage system and supplied to the following crop. This practice again reduces infiltration but also the need of irrigation water.

The availability of protected agriculture maps will improve the conceptualization of transport processes of agricultural contaminants in the regulatory context (EFSA, 2014). In fact, greenhouses are considered closed environments, and for this, the use of banned plant protection products is allowed (PAN Europe, 2023). However, the contamination of surface water with such banned chemicals was confirmed in monitoring studies targeting high-tech greenhouses with hydroponic systems (Boye et al., 2022; PAN Europe, 2023). Garcia-Caparros et al. (2017) report the issue of nitrate leaching from low-tech soil-bound greenhouse crops. Finally, la Cecilia et al. (2021; 2022) conclude that greenhouse systems contradict the expectation of the concurrence of contaminant concentration and load peaks with rain events since rain cannot generate runoff below the greenhouses, but only from crops. Finally, the map of protected agriculture can be used to pinpoint the sources of agricultural plastic (Borg and Camilleri-Fenech, 2024), and improve its waste management when needed.

5. Conclusions

In this research, we developed a novel pan-European protected agriculture map relative to the summer of 2019. Based on the availability of Sentinel-2 data, protected agriculture maps can be created from 2016 onward worldwide. In Europe, the largest extensions of protected agriculture are in Turkey, Spain and Italy. Plastic greenhouses are found to be highly present along Mediterranean coasts and in small islands. Yet, large clusters of high-tech greenhouses are present in northern Europe, such as The Netherlands and Belgium. Greenhouse horticulture food production has been found in other researches in China, North Africa and South America. The method developed here is capable of mapping such locations. However, the workflow necessitates methodological improvements to disregard misclassification issues mainly related to calcium carbonate-rich bare soils and highly reflective anthropic land covers, which lead to an overestimation of protected agriculture. The output map can reveal hotspots where the traditional hydrological and contaminant transport knowledge would fail due to the peculiarity of processes concerning greenhouse horticulture. The results also have direct implications for policymakers aiming to formulate region-specific agricultural and environmental policies. The ability to periodically estimate the extent of protected agriculture enhances the adaptability of policies to changing agricultural landscapes.

CRediT authorship contribution statement

Daniele la Cecilia: Writing – review & editing, Writing – original draft, Visualization, Validation, Software, Resources, Project administration, Methodology, Investigation, Funding acquisition, Formal analysis, Data curation, Conceptualization. **Francesca Despini:** Writing – review & editing, Writing – original draft, Validation, Methodology, Investigation, Formal analysis.

Code availability

The original code of the classification workflow is uploaded with the file name "GEE_OPAC_CloudScorePlus_SORTv2_Country_cicciTurkey_dlc.txt" on the Research Data Unipd repository at 10.25430/researchdata.cab.unipd.it.00001202 (la Cecilia, 2024).

Ethical statement

The authors declare that all ethical practices have been followed in relation to the development, writing and publication of the work reported in this paper

Financial support

This research was complimentary to the project REWATERING and received funding from the European Union's Horizon Europe research and innovation programme under the Marie Skłodowska-Curie grant agreement No. 101062255.

Declaration of competing interest

The authors declare that they have no known competing financial interests or personal relationships that could have appeared to influence the work reported in this paper.

Acknowledgements

This publication was prepared using European Union's Copernicus Land Monitoring Service information (https://doi.org/10.2909/960998c1-1870-4e82-8051-6485205ebbac). We acknowledge the European Space Agency and the Copernicus Program for free and open Sentinel-2 data. The images from Tong et al. (2024a,b) used in this article were downloaded at https://zenodo.org/records/10907151, or viewed at https://rs-cph.projects.earthengine.app/view/greenhouse, and such images were only possible thank to 'Planet Labs PBC'. We thank Benjamin Mary and Miguel Ángel Herrezuelo Bermúdez of the Instituto de Ciencias Agracias (CSIC, Madrid) for the heads-up on the calcareous formations in Spain. We thank the enriching comments from the three anonymous reviewers on previous versions of the manuscript.

Data availability

The training set used to develop OPAC is available at https://doi.org/10.25678/0008NJ (la Cecilia et al., 2023b) and at 10.25430/researchdata.cab.unipd.it.00001202(la Cecilia, 2024).

Data described in this manuscript can be accessed at Research Data Unipd under 10.25430/researchdata.cab.unipd.it.00001202 (la Cecilia, 2024). The data include:•

The 116 output raster files (in EPSG: 4326) with a spatial resolution of 20 m for the year 2019 produced and analysed in this study in geotiff format. The self-explanatory file names are composed by the abbreviated name of the country, the string "GEE_OPAC_Corine-", followed by a string generated by the GEE platform during export. The size of each raster depended on the size of the tiles automatically produced by the GEE platform during export.

The value of each pixel corresponds to one of the following classes:
1Forest,2
Protected Agriculture (classes 2, 3 and 6 were grouped together),4
Shadow,5
Snow7
Vegetated,8
Water,9
Reflective baresoil,10
Baresoil.•

The ESRI shapefile "Validation_all_shape.shp" and related files (in EPSG: 4326) locating the 450 points used for validation. The attribute table consists of:

"ID" - Numeric increasing value for ordering,

"Label" - True label assigned from visual inspection of the true color image from Sentinel-2 and the very high resolution RGB satellite images available in the GEE platform,

"Country" – Country where the pixel belong,

"Long" – Longitude,

"Lat" – Latitude,

"OPAC" – class assigned by the classifier.•

The.csv file containing the additional training dataset extracted from misclassified "protected agricultural" pixels from Turkey for a new version of OPAC to map highly reflective soils.

References

Acharki, S., Kozhikkodan Veettil, B., 2023. Mapping plastic-covered greenhouse farming areas using high-resolution PlanetScope and RapidEye imagery: studies from Loukkos perimeter (Morocco) and Dalat City (Vietnam). Environ. Sci. Pollut. Res. 30, 23012–23022. https://doi.org/10.1007/s11356-022-23808-w.

Achour, Y., Ouammi, A., Zejli, D., 2021. Technological progresses in modern sustainable greenhouses cultivation as the path towards precision agriculture. Renew. Sustain. Energy Rev. 147, 111251. https://doi.org/10.1016/j.rser.2021.111251.

Agüera, F., Aguilar, M.A., Aguilar, F.J., 2006. Detecting greenhouse changes from QuickBird imagery on the Mediterranean coast. Int. J. Rem. Sens. 27, 4751–4767. https://doi.org/10.1080/01431160600702681.

Agüera, F., Aguilar, F.J., Aguilar, M.A., 2008. Using texture analysis to improve per-pixel classification of very high resolution images for mapping plastic greenhouses. ISPRS J. Photogrammetry Remote Sens. 63, 635–646. https://doi.org/10.1016/j.isprsjprs.2008.03.003.

Aguilar, M.A., Vallario, A., Aguilar, F.J., Garcia Lorca, A., Parente, C., 2015. Object-based greenhouse horticultural crop identification from multi-temporal satellite imagery: a case study in Almeria, Spain. Remote Sens. 7, 7378–7401. https://doi.org/10.3390/rs70607378.

AQUASTAT, 2020. Accessed on January 2024 from https://data.apps.fao.org/aquastat/?lang=en&share=f-01d11e7b-68b3-4b32-9c82-345cfadcc890.

Badji, A., Benseddik, A., Bensaha, H., Boukhelifa, A., Hasrane, I., 2022. Design, technology, and management of greenhouse: a review. J. Clean. Prod. 373, 133753. https://doi.org/10.1016/j.jclepro.2022.133753.

Baille, A., Kittas, C., Katsoulas, N., 2001. Influence of whitening on greenhouse microclimate and crop energy partitioning. Agric. For. Meteorol. 107, 293–306.

Balcik, F.B., Senel, G., Goksel, C., 2020. Object-based classification of greenhouses using Sentinel-2 MSI and SPOT-7 images: a case study from Anamur (Mersin), Turkey. IEEE J. Sel. Top. Appl. Earth Obs. Rem. Sens. 13, 2769–2777. https://doi.org/10.1109/JSTARS.2020.2996315.

Batjes, N.H., 2016. Harmonized soil property values for broad-scale modelling (WISE30sec) with estimates of global soil carbon stocks. Geoderma 269, 61–68. https://doi.org/10.1016/j.geoderma.2016.01.034.

Birk, S., Chapman, D., Carvalho, L., et al., 2020. Impacts of multiple stressors on freshwater biota across spatial scales and ecosystems. Nat Ecol Evol 4, 1060–1068. https://doi.org/10.1038/s41559-020-1216-4.

Borg, R., Camilleri-Fenech, M., 2024. Investigating the agricultural use and disposal of plastics in Malta. Sustainability 16, 954. https://doi.org/10.3390/su16030954.

Boye, K., Boström, G., Jonsson, O., Gönczi, M., Löfkvist, K., Kreuger, J., 2022. Greenhouse production contributes to pesticide occurrences in Swedish streams. Sci. Total Environ. 809, 152215. https://doi.org/10.1016/j.scitotenv.2021.152215.

Briassoulis, D., Dougka, G., Dimakogianni, D., Vayas, I., 2016. Analysis of the collapse of a greenhouse with vaulted roof. Biosyst. Eng. 151, 495–509. https://doi.org/10.1016/j.biosystemseng.2016.10.018.

Brown, C.F., Brumby, S.P., Guzder-Williams, B., et al., 2022. Dynamic World, Near realtime global 10 m land use land cover mapping. Sci. Data 9, 251. https://doi.org/10.1038/s41597-022-01307-4.

Bullock, J.M., Aronson, J., Newton, A.C., Pywell, R.F., Rey Benayas, J.M., 2011. Restoration of ecosystem services and biodiversity: conflicts and opportunities. Trends Ecol. Evol. 26, 541–549. https://doi.org/10.1016/j.tree.2011.06.011.

Calero, J., Aranda, V., Montejo-Ráez, A., Martín-García, J.M., 2018. A new soil quality index based on morpho-pedological indicators as a site-specific web service applied to olive groves in the Province of Jaen (South Spain). Comput. Electron. Agric. 146, 66–76. https://doi.org/10.1016/j.compag.2018.01.016.

Campos, J.C., Alírio, J., Arenas-Castro, S., Duarte, L., Garcia, N., Regos, A., Pôças, I., Teodoro, A.C., Sillero, N., 2024. Dynamic shifts of functional diversity through climate-resilient strategies and farmland restoration in a mountain protected area. J. Environ. Manag. 366, 121622. https://doi.org/10.1016/j.jenvman.2024.121622.

Carroll, M., DiMiceli, C., Wooten, M., Hubbard, A., Sohlberg, R., Townshend, J., 2017. MOD44W MODIS/terra land water mask derived from MODIS and SRTM L3 global 250m SIN grid V006 [data set]. NASA EOSDIS Land Processes Distributed Active Archive Center. https://doi.org/10.5067/MODIS/MOD44W.006, 2023-10-13.

Castro, A.J., López-Rodríguez, M.D., Giagnocavo, C., Gimenez, M., Céspedes, L., La Calle, A., Gallardo, M., Pumares, P., Cabello, J., Rodríguez, E., et al., 2019. Six collective challenges for sustainability of Almería greenhouse horticulture. Int. J. Environ. Res. Publ. Health 16, 4097. https://doi.org/10.3390/ijerph16214097.

CORINE Land Cover 2018 (raster 100 m). European Union's Copernicus Land Monitoring Service information. Accessed in the Google Earth Engine at https://developers.google.com/earth-engine/datasets/catalog/COPERNICUS_CORINE_V20_100m#description, doi: 10.2909/960998c1-1870-4e82-8051-6485205ebbac.

de Souza, M.F., Lamparelli, R.A.C., Oliveira, M.H.S., et al., 2024. Remote sensing detection of plastic-mulched farmland using a temporal approach in machine learning: case study in tomato crops. Environ. Sci. Pollut. Res. https://doi.org/10.1007/s11356-024-35026-7.

Defourny, P., Bontemps, S., Bellemans, N., et al., 2019. Near real-time agriculture monitoring at national scale at parcel resolution: Performance assessment of the Sen2-Agri automated system in various cropping systems around the world. Remote Sens Environ 221, 551–568. https://doi.org/10.1016/j.rse.2018.11.007.

Dekker, R.J., 2003. Texture analysis and classification of ERS SAR images for map updating of urban areas in The Netherlands. IEEE Trans. Geosci. Rem. Sens. 41, 1950–1958. https://doi.org/10.1109/TGRS.2003.814628.

Demuzere, M., Kittner, J., Martilli, A., Mills, G., Moede, C., Stewart, I.D., van Vliet, J., Bechtel, B., 2022. A global map of local climate zones to support earth system modelling and urban-scale environmental science. Earth Syst. Sci. Data 14, 3835–3873. https://doi.org/10.5194/essd-14-3835-2022.

Duru, M., Therond, O., Martin, G., et al., 2015. How to implement biodiversity-based agriculture to enhance ecosystem services: a review. Agron. Sustain. Dev. 35, 1259–1281. https://doi.org/10.1007/s13593-015-0306-1.

EFSA, 2014. EFSA Guidance Document on clustering and ranking of emissions of active substances of plant protection products and transformation products of these active substances from protected crops (greenhouses and crops grown under cover) to relevant environmental compartments. EFSA J. 12, 43. https://doi.org/10.2903/j.efsa.2014.3615.

Erb, K.H., Lauk, C., Kastner, T., et al., 2016. Exploring the biophysical option space for feeding the world without deforestation. Nat. Commun. 7, 11382. https://doi.org/10.1038/ncomms11382.

FAO, 2015. FAO GAUL: global administrative unit layers 2015, country boundaries. Accessed on the Google Earth Engine platform and available at https://data.apps.fao.org/map/catalog/srv/eng/catalog.search?id=12691#/home.

Espí, E., Salmerón, A., Fontecha, A., García, Y., Real, A.I., 2006. Plastic films for agricultural applications. J. Plastic Film Sheeting 22 (2), 85–102. https://doi.org/10.1177/8756087906064220.

FAO, 2022. Land Use Statistics and Indicators. Global, Regional and Country Trends – 2000–2020. FAOSTAT Analytical Brief, Rome. https://doi.org/10.4060/cc0963en, 48.

Farr, T.G., Rosen, P.A., Caro, E., Crippen, R., Duren, R., Hensley, S., Kobrick, M., Paller, M., Rodriguez, E., Roth, L., Seal, D., Shaffer, S., Shimada, J., Umland, J., Werner, M., Oskin, M., Burbank, D., Alsdorf, D.E., 2007. The shuttle radar topography mission. Rev. Geophys. 45, RG2004. https://doi.org/10.1029/2005RG000183.

Fernández, M.D., Bonachela, S., Orgaz, F., Thompson, R., López, J.C., Granados, M.R., Gallardo, M., Fereres, E., 2010. Measurement and estimation of plastic greenhouse reference evapotranspiration in a Mediterranean climate. Irrig Sci 28, 497–509. https://doi.org/10.1007/s00271-010-0210-z.

Filippa, G., Cremonese, E., Galvagno, M., et al., 2022. On the distribution and productivity of mountain grasslands in the Gran Paradiso National Park, NW Italy: a remote sensing approach. Int. J. Appl. Earth Obs. Geoinf. 108, 102718. https://doi.org/10.1016/j.jag.2022.102718.

Foley, J.A., DeFries, R., Asner, G.P., Barford, C., Bonan, G., Carpenter, S.R., Chapin, F.S., Coe, M.T., Daily, G.C., Gibbs, H.K., Helkowski, J.H., Holloway, T., Howard, E. A., Kucharik, C.J., Monfreda, C., Patz, J.A., Prentice, I.C., Ramankutty, N., Snyder, P.K., 2005. Global consequences of land use. Science 309, 570–574. https://doi.org/10.1126/science.1111772.

Gallagher, T.M., Breecker, D.O., 2020. The obscuring effects of calcite dissolution and formation on quantifying soil respiration. Glob. Biogeochem. Cycles 34, e2020GB006584. https://doi.org/10.1029/2020GB006584.

Gao, B.-C., 1996. NDWI—a normalized difference water index for remote sensing of vegetation liquid water from space. Rem. Sens. Environ. 58, 257–266. https://doi.org/10.1016/S0034-4257(96)00067-3.

Garcia-Caparros, P., Contreras, J.I., Baeza, R., Segura, M.L., Lao, M.T., 2017. Integral management of irrigation water in intensive horticultural systems of Almería. Sustainability 9, 2271. https://doi.org/10.3390/su9122271.

Goddek, S., Körner, O., Keesman, K.J., Tester, M.A., Lefers, R., Fleskens, L., Joyce, A., van Os, E., Gross, A., Leemans, R., 2023. How greenhouse horticulture in arid regions can contribute to climate-resilient and sustainable food security. Glob. Food Secur. 100701. https://doi.org/10.1016/j.gfs.2023.100701.

Gorelick, N., Hancher, M., Dixon, M., Ilyushchenko, S., Thau, D., Moore, R., 2017. Google earth engine: planetary-scale geospatial analysis for everyone. Remote Sens. Environ. 202, 18–27. https://doi.org/10.1016/j.rse.2017.06.031.

Habel, J.C., Dengler, J., Janišová, M., Török, P., Wellstein, C., Wiezik, M., 2013. European grassland ecosystems: threatened hotspots of biodiversity. Biodivers. Conserv. 22, 2131–2138. https://doi.org/10.1007/s10531-013-0537-x.

Ibrahim, E., Gobin, A., 2021. Sentinel-2 recognition of uncovered and plastic covered agricultural soil. Remote Sens. 13, 4195. https://doi.org/10.1016/j.jag.2024.103829.

Jägermeyr, J., Pastor, A., Biemans, H., Gerten, D., 2017. Reconciling irrigated food production with environmental flows for Sustainable Development Goals implementation. Nat. Commun. 8, 15900. https://doi.org/10.1038/ncomms15900.

Jiménez-Lao, R., Aguilar, F.J., Nemmaoui, A., Aguilar, M.A., 2020. Remote sensing of agricultural greenhouses and plastic-mulched farmland: an analysis of worldwide research. Remote Sens. 12, 2649. https://doi.org/10.3390/rs12162649.

Khanal, S., Kc, K., Fulton, J.P., Shearer, S., Ozkan, E., 2020. Remote sensing in agriculture—accomplishments, limitations, and opportunities. Remote Sens. 12, 3783. https://doi.org/10.3390/rs12223783.

Koc-San, D., 2013. Evaluation of different classification techniques for the detection of glass and plastic greenhouses from WorldView-2 satellite imagery. J. Appl. Remote Sens. 7, 073553. https://doi.org/10.1117/1.JRS.7.073553.

la Cecilia, D., 2024. Data for: periodic protected agriculture mapping at continental scales with Sentinel-2 imagery within the Google Earth Engine platform. Research Data Unipd. https://doi.org/10.25430/researchdata.cab.unipd.it.00001202 [Data set].

la Cecilia, D., Camporese, M., 2022. Resolving streamflow diel fluctuations in a small agricultural catchment with an integrated surface-subsurface hydrological model. Hydrol. Process. 36, e14768. https://doi.org/10.1002/hyp.14768.

la Cecilia, D., Dax, A., Ehmann, H., Koster, M., Singer, H., Stamm, C., 2021. Continuous high-frequency pesticide monitoring to observe the unexpected and the overlooked. Water Res. X 13, 100125. https://doi.org/10.1016/j.wroa.2021.100125.

la Cecilia, D., Dax, A., Ehmann, H., Koster, M., Singer, H., Stamm, C., 2022. Continuous high-frequency pesticide monitoring in a small tile-drained agricultural stream to reveal diel concentration fluctuations in dry periods. Front. Water. https://doi.org/10.3389/frwa.2022.1062198.

la Cecilia, D., Tom, M., Stamm, C., Odermatt, D., 2023a. Pixel-based mapping of open field and protected agriculture using constrained Sentinel-2 data, ISPRS Open J. Photogramm. Remote Sens. 8, 100033. https://doi.org/10.1016/j.ophoto.2023.100033.

la Cecilia, D., Tom, M., Stamm, C., Odermatt, D., 2023b. Data for: pixel-based mapping of open field and protected agriculture using constrained Sentinel-2 data (Version 1.0). Eawag: Swiss Federal Institute of Aquatic Science and Technology. https://doi.org/10.25678/0008NJ [Data set].

la Cecilia, D., Venezia, A., Maino, D., Camporese, M., 2024. Towards an understanding of the hydrological processes of greenhouse horticulture districts. EGU General Assembly, 2024. https://doi.org/10.5194/egusphere-egu24-9140. Vienna, Austria, 14–19 Apr 2024, EGU24-9140.

Lanorte, A., De Santis, F., Nolè, G., Blanco, I., Loisi, R.V., Schettini, E., Vox, G., 2017. Agricultural plastic waste spatial estimation by Landsat 8 satellite images. Comput. Electron. Agric. 141, 35–45. https://doi.org/10.1016/j.compag.2017.07.003.

Locatelli, S., Barrera, W.Jr., Verdi, L., Nicoletto, C., Dalla Marta, A., Maucieri, C., 2024. Modelling the response of tomato on deficit irrigation under greenhouse conditions. Sci. Horti. 326, 112770. https://doi.org/10.1016/j.scienta.2023.112770.

Ma, A., Chen, D., Zhong, Y., Zheng, Z., Zhang, L., 2021. National-scale greenhouse mapping for high spatial resolution remote sensing imagery using a dense object dual-task deep learning framework: a case study of China. ISPRS J. Photogrammetry Remote Sens. 181, 279–294. https://doi.org/10.1016/j.isprsjprs.2021.08.02.

Maggi, F., Tang, F.H.M., la Cecilia, D., McBratney, A., 2019. PEST-CHEMGRIDS, global gridded maps of the top 20 crop-specific pesticide application rates from 2015 to 2025. Sci. Data 6, 170. https://doi.org/10.1038/s41597-019-0169-4.

Messelink, G.J., Lambion, J., Janssen, A., van Rijn, P.C.J., 2021. Biodiversity in and around greenhouses: benefits and potential risks for pest management. Insects 12, 933. https://doi.org/10.3390/insects12100933.

Modanesi, S., Massari, C., Gruber, A., Lievens, H., Tarpanelli, A., Morbidelli, R., De Lannoy, G.J.M., 2021. Optimizing a backscatter forward operator using Sentinel-1 data over irrigated land. Hydrol. Earth Syst. Sci. 25, 6283–6307. https://doi.org/10.5194/hess-25-6283-2021.

Nguyen, T.H., Tang, F.H.M., Conchedda, G., Casse, L., Obli-Laryea, G., Tubiello, F.N., Maggi, F., 2024. NPKGRIDS: a global georeferenced dataset of N, P_2O_5, and K_2O fertilizer application rates for 173 crops. Sci. Data 11, 1179. https://doi.org/10.1038/s41597-024-04030-4.

Ou, C., Yang, J., Du, Z., Liu, Y., Feng, Q., Zhu, D., 2019. Long-term mapping of a greenhouse in a typical protected agricultural region using landsat imagery and the google earth engine. Remote Sens. 12, 55. https://doi.org/10.3390/rs12010055.

Ou, C., Yang, J., Du, Z., Zhang, T., Niu, B., Feng, Q., et al., 2021. Landsat-derived annual maps of agricultural greenhouse in Shandong province, China from 1989 to 2018. Remote Sens. 13, 4830. https://doi.org/10.3390/rs13234830.

PAN Europe, 2023. Pesticide action network Europe. Report: "it rains pesticides from greenhouses. The End of a Myth, Greenhouses Are Releasing Pesticides into the Environment.
Parmeggiani, D., Despini, F., Costanzini, S., Teggi, S., la Cecilia, D., 2024. Hyperspectral analysis for protected agriculture land cover mapping: a remote sensing approach (No. EGU24-10884). Copernicus Meetings. https://doi.org/10.5194/egusphere-egu24-10884.
Pasquarella, V.J., Brown, C.F., Czerwinski, W., Rucklidge, W.J., 2023. Comprehensive quality assessment of optical satellite imagery using weakly supervised video learning. IEEE/CVF Conference on Computer Vision and Pattern Recognition Workshops (CVPRW), pp. 2125–2135. https://doi.org/10.1109/CVPRW59228.2023.00206. Vancouver, BC, Canada.
Perilla, G.A., Mas, J.F., 2019. High-resolution mapping of protected agriculture in Mexico, through remote sensing data cloud geoprocessing. Eur. J. Remote Sens. 52, 532–541. https://doi.org/10.1080/22797254.2019.1686430.
Pörtner, H.O., Scholes, R.J., Agard, J., et al., 2021. IPBES-IPCC co-sponsored workshop report on biodiversity and climate change. IPBES and IPCC. https://doi.org/10.5281/zenodo.478253.
Rey Benayas, J.M., Bullock, J.M., 2012. Restoration of biodiversity and ecosystem services on agricultural land. Ecosystems 15, 883–899. https://doi.org/10.1007/s10021-012-9552-0.
Rosa, L., Chiarelli, D.D., Rulli, M.C., Dell'Angelo, J., D'Odorico, P., 2020. Global agricultural economic water scarcity. Sci. Adv. 6, eaaz6031. https://doi.org/10.1126/sciadv.aaz6031.
Rouse, J.W., Haas, R.H., Schell, J.A., Deering, D.W., 1974. Monitoring vegetation systems in the great plains with ERTS. In: Freden, S.C., Mercanti, E.P., Becker, M. (Eds.), Third Earth Resources Technology Satellite–1 symposium.Volume I: Technical Presentations, NASA SP-351. NASA, Washington, D.C, pp. 309–317.
Ryken, A.C., Gochis, D., Maxwell, R.M., 2022. Unravelling groundwater contributions to evapotranspiration and constraining water fluxes in a high-elevation catchment. Hydrol. Process. 36, e14449. https://doi.org/10.1002/hyp.14449.
Santos-Francés, F., Martínez-Graña, A., Ávila-Zarza, C., Criado, M., Sánchez-Sánchez, Y., 2022. Soil quality and evaluation of spatial variability in a semi-arid ecosystem in a region of the southeastern iberian peninsula (Spain). Land 11, 5. https://doi.org/10.3390/land11010005.
Santunione, G., Libbra, A., Muscio, A., 2017. Cool roofs with high solar reflectance for the welfare of dairy farming animals. J. Phys. Conf. 796, 012028. https://doi.org/10.1088/1742-6596/796/1/012028.
Schils, R.L.M., Bufe, C., Rhymer, C.M., et al., 2022. Permanent grasslands in Europe: land use change and intensification decrease their multifunctionality. Agric. Ecosyst. Environ. 330, 107891. https://doi.org/10.1016/j.agee.2022.107891.
Segarra, J., Buchaillot, M.L., Araus, J.L., Kefauver, S.C., 2020. Remote sensing for precision agriculture: Sentinel-2 improved features and applications. Agronomy 10, 641. https://doi.org/10.3390/agronomy10050641.
Simou, M.R., Loulad, S., Aamir, Z., Maanan, M., Rhinane, H., 2023. Using YOLOV5 to detect plastic greenhouses in Morocco. Int. Arch. Photogram. Rem. Sens. Spatial Inf. Sci. 48, 351–354. https://doi.org/10.5194/isprs-archives-XLVIII-4-W6-2022-351-2023.
Sishodia, R.P., Ray, R.L., Singh, S.K., 2020. Applications of remote sensing in precision agriculture: a review. Remote Sens. 12, 3136. https://doi.org/10.3390/rs12193136.
Steven, M.D., Clark, J.A. (Eds.), 2013. Applications of Remote Sensing in Agriculture. Elsevier.
Tong, X., Zhang, X., Fensholt, R., et al., 2024a. Global area boom for greenhouse cultivation revealed by satellite mapping. Nat. Food 5, 513–523. https://doi.org/10.1038/s43016-024-00985-0.
Tong, X., Brandt, M., Fensholt, R., 2024b. Global-scale greenhouse cultivation areas (Version 1). Zenodo. https://doi.org/10.5281/zenodo.10907151 [Data set].
Tsendbazar, N., Herold, M., Li, L., Tarko, A., de Bruin, S., Masiliunas, D., Duerauer, M., 2021. Towards operational validation of annual global land cover maps. Rem. Sens. Environ. 266. https://doi.org/10.1016/j.rse.2021.112686.
Wade, C.M., Baker, J.S., Van Houtven, G., Cai, Y., Lord, B., Castellanos, E., Leiva, B., Fuentes, G., Alfaro, G., kondash, A.J., henry, C.L., Shaw, B., Redmon, J.H., 2022. Opportunities and spatial hotspots for irrigation expansion in Guatemala to support development goals in the food-energy-water nexus. Agric. Water Manag. 267, 107608. https://doi.org/10.1016/j.agwat.2022.107608.
Wang, Q., Chen, W., Tang, H., Pan, X., Zhao, H., Yang, B., et al., 2023. Simultaneous extracting area and quantity of agricultural greenhouses in large scale with deep learning method and high-resolution remote sensing images. Sci. Total Environ. 872, 162229. https://doi.org/10.1016/j.scitotenv.2023.162229.
Weiss, M., Jacob, F., Duveiller, G., 2020. Remote sensing for agricultural applications: a meta-review. Remote Sens. Environ. 236, 111402. https://doi.org/10.1016/j.rse.2019.111402.
Wójtowicz, M., Wójtowicz, A., Piekarczyk, J., 2016. Application of remote sensing methods in agriculture. Commun. Biometry Crop. Sci. 11, 31–50.
Yang, D., Huang, X., 2024. Landscape design and planning methods for plant protection based on deep learning and remote sensing techniques. Crop Prot., 106620 https://doi.org/10.1016/j.cropro.2024.106620.
Zanaga, D., Van De Kerchove, R., De Keersmaecker, W., Souverijns, N., Brockmann, C., Quast, R., Wevers, J., Grosu, A., Paccini, A., Vergnaud, S., Cartus, O., Santoro, M., Fritz, S., Georgieva, I., Lesiv, M., Carter, S., Herold, M., Li, Linlin, Tsendbazar, N.E., Ramoino, F., Arino, O., 2021. ESA WorldCover 10 M 2020 V100. https://doi.org/10.5281/zenodo.5571936.
Zhang, R., Wang, L., Khalizov, A.F., Molina, L.T., 2009. Formation of nanoparticles of blue haze enhanced by anthropogenic pollution. Proc. Natl. Acad. Sci. USA 106, 17650–17654. https://doi.org/10.1073/pnas.0910125106.
Zhang, P., Du, P., Guo, S., Zhang, W., Tang, P., Chen, J., Zheng, H., 2022. A novel index for robust and large-scale mapping of plastic greenhouse from Sentinel-2 images. Remote Sens. Environ. 276, 113042. https://doi.org/10.1016/j.rse.2022.113042.
Zhou, D., Meinke, H., Wilson, M., Marcelis, L.F.M., Heuvelink, E., 2021. Towards delivering on the sustainable development goals in greenhouse production systems. Resour. Conserv. Recycl. 169, 105379. https://doi.org/10.1016/j.resconrec.2020.105379.
Zhou, S., Kaufmann, H., Bohn, N., Bochow, M., Kuester, T., Segl, K., 2022. Identifying distinct plastics in hyperspectral experimental lab-, aircraft-, and satellite data using machine/deep learning methods trained with synthetically mixed spectral data. Remote Sens. Environ. 281, 113263. https://doi.org/10.1016/j.rse.2022.113263.